Petroleum Research xxx (xxxx) xxx

Contents lists available at ScienceDirect

Petroleum Research

journal homepage: http://www.keaipublishing.com/en/journals/petroleum-research/

Prediction of abnormal pressure from AVO velocities over "Safety" field, onshore Niger delta, Nigeria

O. Abiola*, T.G. Ayenuro

Department of Applied Geophysics, Federal University of Technology, Akure, Nigeria

ARTICLE INFO

Article history:
Received 22 June 2020
Received in revised form
16 September 2020
Accepted 16 September 2020
Available online xxx

Keywords:
Abnormal pressure
Amplitude variation with offset
Velocities information
Pore pressure
Disequilibrium compaction

ABSTRACT

Abnormal pressure prediction was undertaken in "Safety" field, onshore Niger Delta, Nigeria using amplitude variation with offset (AVO) velocities information. Each of the methods used form an integral part of a process that produces AVO Analysis, AVO velocity inversion, extraction of seismic velocity from AVO velocities inversion results and pore pressure prediction. Pore pressure predicted from the seismic velocity has a better resolution than the pressure predicted from the interval transit time. The pore pressure within the field ranges from 14.7psi to 3916psi. Overpressured and underpressured zones were delineated on the field from the pressure predicted from the seismic velocities. Within the field, the overpressured zones were delineated at depth 6855 ft–7802 ft. Over pressure top was delineated at a depth of 6855 ft with a pore pressure of 3053psi and a corresponding hydrostatic pressure of 2722psi. The under-pressured zones were also delineated at depth 7883 ft–9288 ft. The under pressure top was delineated at a depth of 7883 ft with a pressure of 1093psi and a corresponding hydrostatic pressure of 3122psi. Porosity values within the over pressure zone ranges from 23% to 53% which could be considered as relatively high. This could be as a result of the fact that the pore fluid cannot be expelled rapidly thereby causing the pore fluid to increase rapidly since they are no longer compacted; thus leading to overpressure. As a result of overpressure top which is directly above the reservoir top within the shale zone, drilling this reservoir vertically could not be suggested so as to avoid possible blow out. It was also observed that the primary cause or mechanism of overpressure within this field could be disequilibrium compaction.

1. Introduction

Continued success in the search for oil and gas reserves depends upon thorough understanding of the subsurface geology of exploration fields (Abiola et al., 2018). Pressure fields, and especially overpressure in petroliferous sags, had significant impacts on hydrocarbon generation, evolution, migration, accumulation and preservation of organic matters (Jiang et al., 2017). Knowledge of pore pressure information in the subsurface is important in planning and designing drilling. To be able to characterize the reservoir of over pressured zones, the lore of the subsurface pore pressure is very important because it has significant impact on seismic rock properties (Li et al., 2007). Abnormal pore pressures is a worldwide problem in oil and gas exploration, often result in drilling problems such as borehole instability, stuck pipe, lost circulation, kicks and even blowouts. Pore pressures are the fluid pressures in the pore spaces in the porous formations which vary from hydrostatic pressure to severe overpressure. When the pore pressure is lower or higher than the hydrostatic pressure (normal pore pressure), it is called abnormal pore pressure and when the pore pressure exceeds or is higher than the normal pressure, it is overpressure or higher pressure and has significant importance in geo-hazards analysis and prediction (Bowers, 2012). In the high over pressured regions, accurate predrill pore pressure prediction is very important for casing point selection and well planning. Pore pressure prediction has an implication in migration modeling for prospect evaluation and seal prediction. The two most common mechanisms of overpressure generation are undercompaction and fluid expansion. Pore pressure prediction schemes required for both mechanisms are different, as their effect on rock properties are not the same (Tingay et al., 2009). The undercompaction is the main mechanism of overpressure generation in most of the Tertiary sedimentary basins where sedimentation rate is high. Other mechanisms such as

* Corresponding author.
E-mail address: oabiola@futa.edu.ng (O. Abiola).

https://doi.org/10.1016/j.ptlrs.2020.09.002

Fig. 1. Location of the Niger Delta and the study area (Odunayo and Ehinola, 2010).

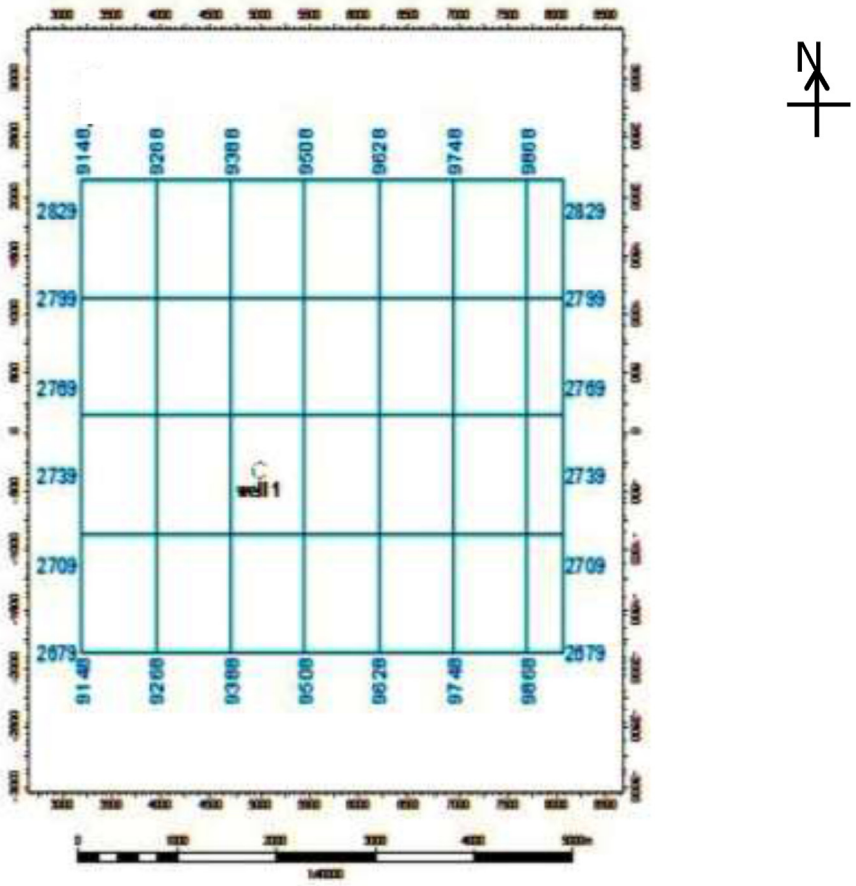

Fig. 2. Base map of the study area showing the well location.

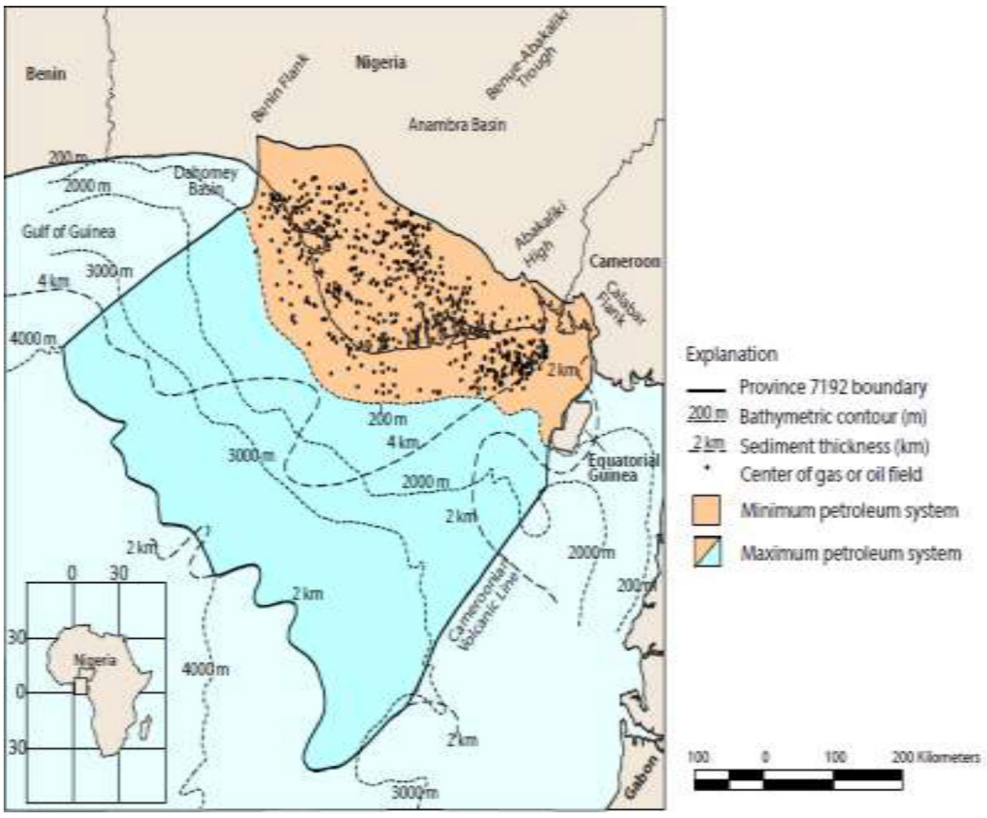

Fig. 3. Map of the Niger Delta showing province outline (Tuttle et al., 1999).

chemical compaction and fluid expansion can generate overpressure in the deeper part of the sedimentary basins (Deming et al., 2002). For pore pressure prediction, understanding the different mechanisms of overpressure generation and their effect on rock properties are very important (Swarbrick, 2001). Seismic velocity is most reliable tool for predrill pore pressure prediction in the frontier area. Seismic pressure prediction relies on detecting changes in interval velocity with depth. Alteration in the properties of overpressured rocks is a reflection of changes in the interval velocity with depth, which, in most cases, are undercompacted

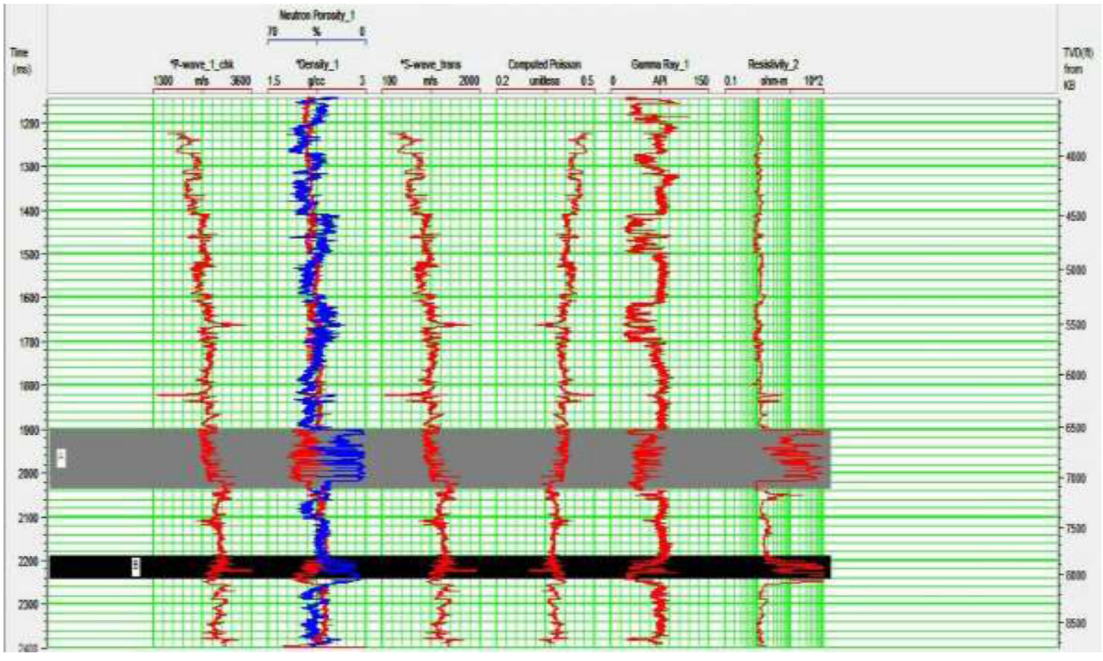

Fig. 4. Well window showing the composite logs.

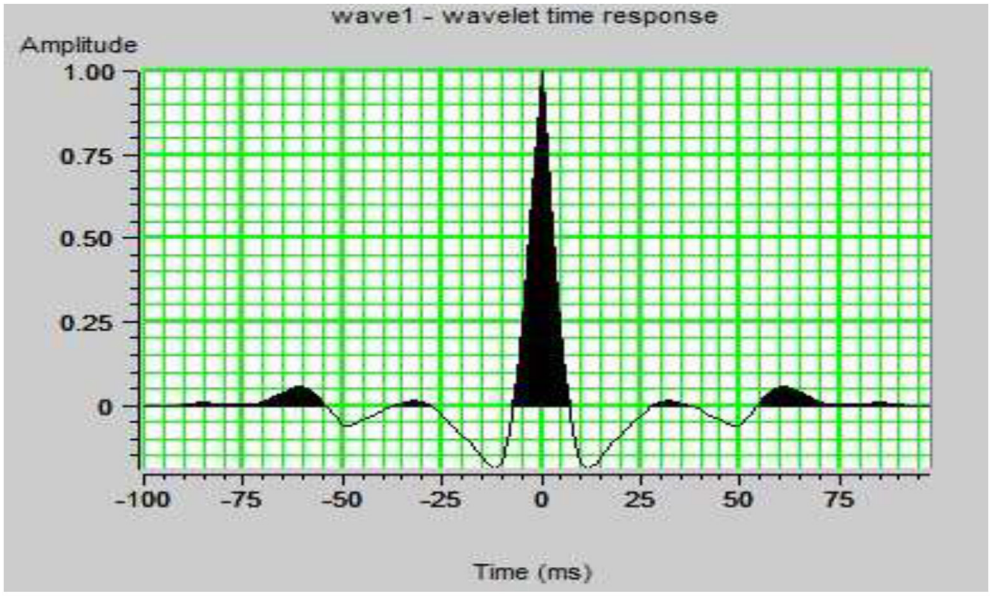

(a)

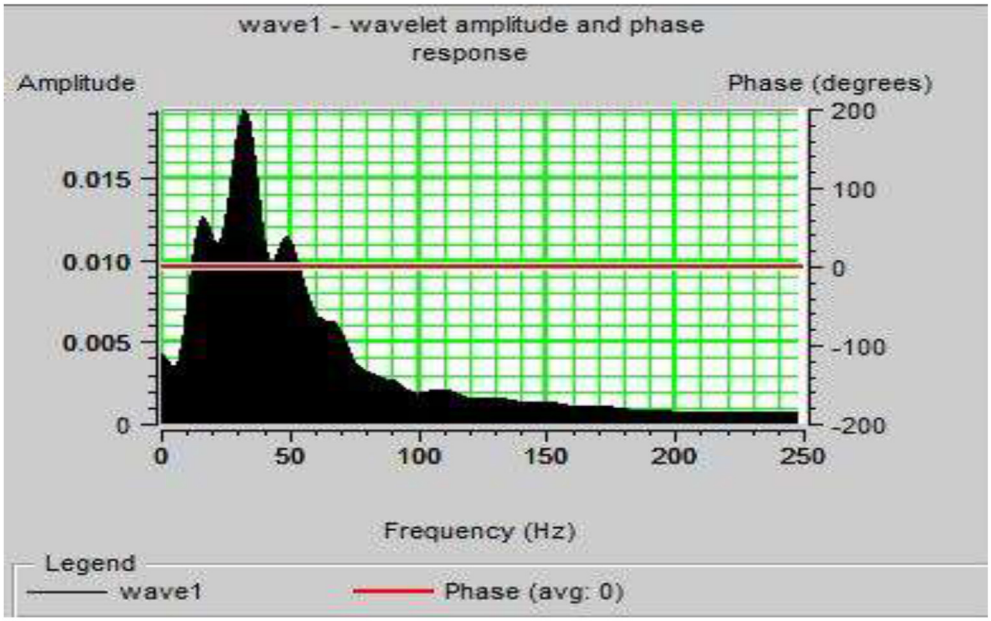

(b)

Fig. 5. (a) Statistical wavelet extraction; (b): Wavelet amplitude and phase response.

(Dutta, 2002). Mechanical compaction due to sedimentation increases the effective stress and reduces the porosity with depth. Seismic P-wave velocity has direct relation with effective stress and increase with depth due to increase in effective stress. However, if the rate of sedimentation is very high and the fluid cannot escape from the pore space due to low permeability in rock, the pore fluid will support a part of the overburden and become overpressured. Sayers et al. (2002), reported that seismic velocity could be used in predicting pore pressure as overpressure reduces the amount of compaction that could occur within the subsurface rocks. According to Chopra and Huffman (2006), accuracy of the seismic velocity is one of the key factors required for reliable pore pressure prediction. The quality of the seismic velocity could be improved using advanced seismic processing techniques like high-density - high-resolution velocity analysis, prestack seismic simultaneous inversion, and anisotropic prestack depth migration. Overpressures are usually generated by mechanisms such as compaction disequilibrium (undercompaction), hydrocarbon generation and gas cracking, aquathermal expansion, tectonic compression (lateral stress), mineral transformations (e.g. illitization), and osmosis, hydraulic head and hydrocarbon buoyancy (Gutierrez et al., 2006; Swarbrick and Osborne, 1998). In nearly all cases where compaction disequilibrium has been determined to be the primary cause of overpressuring, the age of the rocks is geologically young. Accurate

pore pressures prediction in overpressured regions is essential to ensure safe drilling operations and reduce the cost of drilling (Abiola et al., 2016). The quantification of pressures is a challenge as there is a great difficulty in measuring pressures at depth, as well as taking cores for geomechanical tests that can help in the analysis of the stress state of the rock and the definition of overpressure generation mechanisms. Typically, the pore pressure predictions use models based on porosity and stress values from well log data that can be used with 2D or 3D seismic data. A pre-drill estimate of pore pressure can be obtained from seismic velocities using a velocity-to pore pressure transform calibrated from offset well data.

2. Geological settings

The study area, "Safety" field (Fig. 1) is situated on the onshore part of Niger Delta, Nigeria within latitudes 3° and 6°N and longitudes 5° and 8°E and the base map for the study area is as shown in Fig. 2. The Niger Delta is situated in the Gulf of Guinea and extends throughout the Niger Delta Province as defined by Klett et al. (1997). From the Eocene to the present, the delta has prograded south-westward, forming depobelts that represent the most active portion of the delta at each stage of its development (Doust and Omatsola, 1989). These depobelts form one of the largest regressive deltas in the world with an area of some 300,000 km^2 (Kulke, 1995), a sediment volume of 500,000 km^3 (Hospers, 1965), and a sediment thickness of over 10 km in the basin depocenter (Kaplan et al., 1994).

The onshore portion of the Niger Delta Province is delineated by the geology of southern Nigeria and southwestern Cameroon (Fig. 3). The northern boundary is the Benin flank-an east-northeast trending hinge line south of the West Africa basement massif (Tuttle et al., 1999). The north eastern boundary is defined by outcrops of the Cretaceous on the Abakaliki High and further east-south-east by the Calabar flank–a hinge line bordering the adjacent Precambrian. The province covers 300,000 km^2 and includes the geologic extent of the Tertiary Niger Delta (Akata-Agbada) petroleum system.

3. Materials and methodology

The materials used for the research work include base map of the study area, 3-D pre-stacked seismic data (near, mid, and far offset partial stacked volumes, and full offset stacked volume) which consists of 161 inlines ranging from 2679 to 2839 and 195 crosslines ranging from 9148 to 9924; normal moveout (NMO) corrected migrated 3-D pre-stack gather volume consisting of 231 common midpoint (CMP) gathers across the entire area, one checkshot data, deviation directional data, suite of wireline logs which include gamma ray, resistivity, sonic, compensated formation density, and neutron porosity logs. The 3-D pre-stack seismic data have been processed already into normal moveout corrected pre-stack migrated near, mid, far offset partial stacks and full offset stack. The common mid-point (CMP) gathers have also been corrected for normal moveout effects and migrated. The corrected CMP gathers are further processed into super gathers. Seismic wavelet was extracted from the pre-stacked seismic data to generate the offset dependent synthetic alongside with the P-wave, Density, and computed S-wave logs. This wavelet is zero phase and has a dominant frequency of about 30 Hz, determined from the seismic data but this does not implies that the seismic data is at zero-phase. The main seismic parameter used for the study is the prestack time migration (PSTM).

3.1. AVO analysis

The data were enhanced to improve the signal to noise ratio by applying multiple and radon noise suppression. The Trim Static process was applied to the multiples and random noise to get rid of the remaining effects of the NMO correction. In the Trim Static process, 20 ms time window was defined to align and shift the trace in the gather. After Trim Static process, it was observed that the signal to noise ratio was improved at the offsets. The logs imported into the well database are sonic, density, gamma, self-potential and

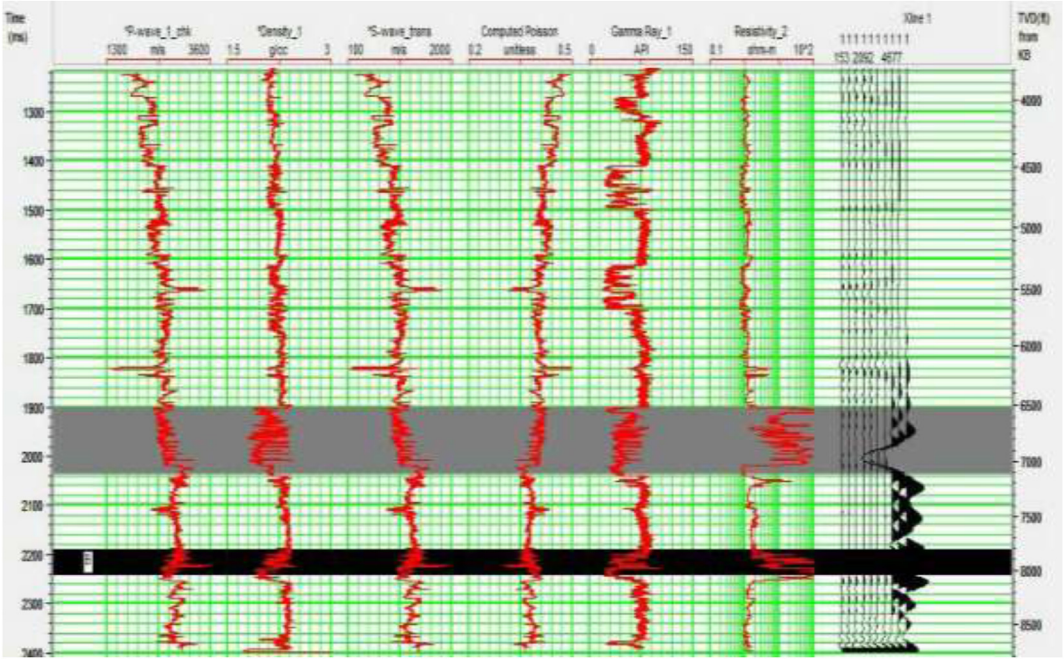

Fig. 6. Zero-offset dependent synthetic.

resistivity logs. The logs were then attached to their corresponding units. The coordinates of the well location and its elevation were also inputed into the well database. The imported well was then used to generate a synthetic, in order to perform this; the well in the database was selected through the modeling process on the AVO interface. The logs available in this well (P-wave and Density logs) were then defined in the synthetic input pane. The S-wave was generated from the P-wave using Castagna's mud rock equation which relates S-wave and P-wave velocity by a linear equation:

$$S_{\text{wave}} = C_1 \times P_{\text{wave}} + C_2 \quad (1)$$

where: $C_1 = 0.86190$, $C_2 = -1172.00$.

The generated S-wave and P-wave were then saved and displayed on the modeling interface. The calculated S-wave using the Castagna's equation can effectively model the entire log as a wet log. In order to calculate the correct S-wave behavior within the reservoir sands, a fluid replacement modeling (FRM) was performed. Three new logs which would later be used to generate the synthetic were generated, including: P-wave-FRM, density-FRM, and S-wave-FRM. The imported 3-D pre-stack data was displayed on the AVO modeling interface. Horizons were mapped across inlines and crosslines of the seismic volume to generate a surface for the interpretation. Super-gather, trim statics and angle gather processes were applied to the data. The first AVO signal process applied to the 3-D pre-stack data was the super-gather. This operation was performed so as to increase effective signal to noise ratio, while maintaining AVO amplitude information as well as to reduce data volume. The seismic super-gather was then displayed at the end of the operation. An operation called trim statics was performed on the resulting super-gather volume. This operation was

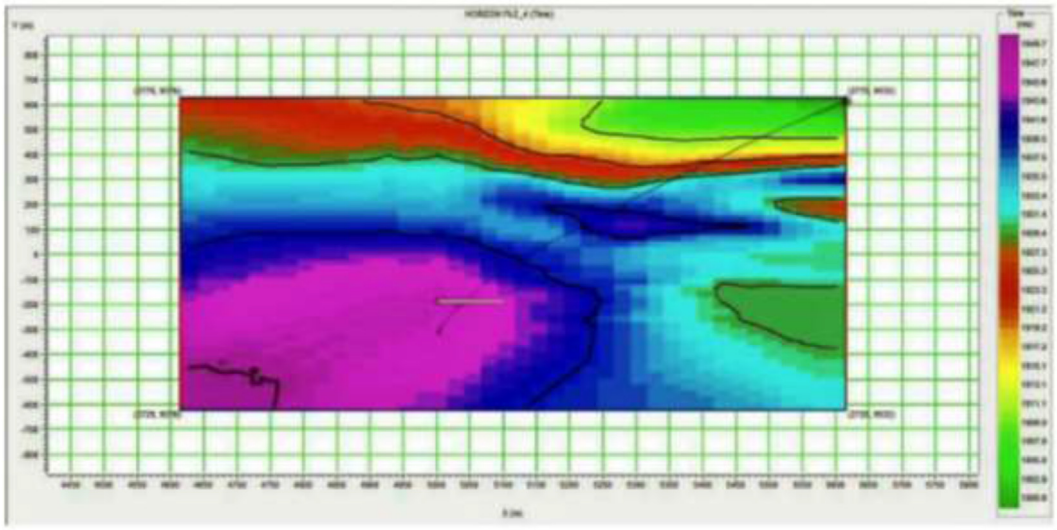

(a)

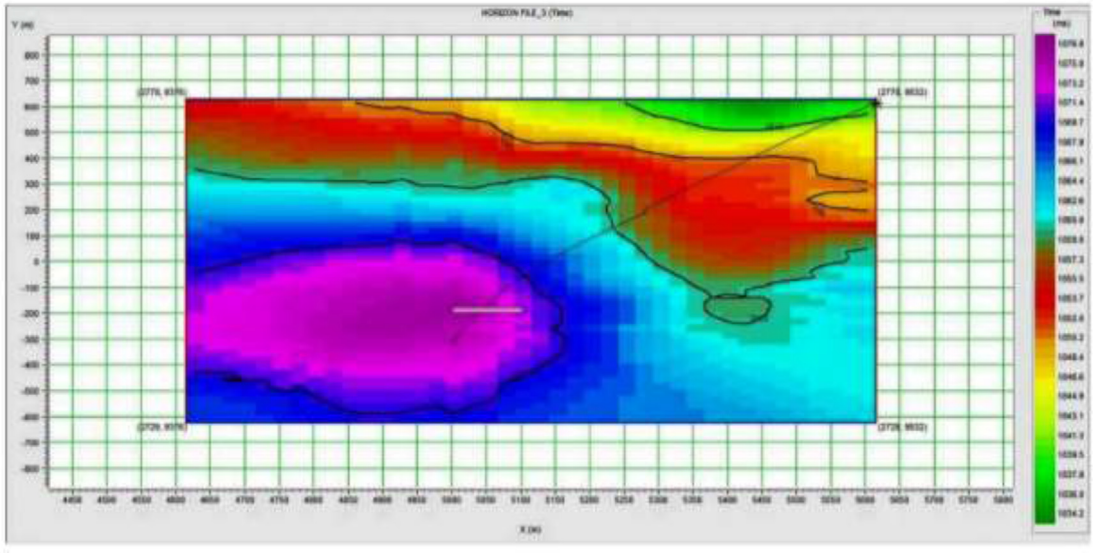

(b)

Fig. 7. (a) Mapped horizon 1; (b) Mapped horizon 2.

carried out so as to remove the problem of residual moveout, via the process tool on AVO modeling interface. The next data processing performed is called the angle gather. The input volume used for this operation is the seismic super-gather volume. The angle gather operation would give a better view of the distribution of the incidence angles at the zone of interest.

3.2. Inversion

Pre-stack inversion operates in incident angle domain, so the first step involves conversion from offset to angle domain. For the conversion process to be successful, a sonic log was imported from the database. A horizon was then imported from the AVO modeling interface. The wavelets used for the inversion was then extracted. The pre-stack inversion allows the use of different wavelets for each angle. This is due to the fact that the frequency-dependent absorption and normal move out (NMO) tuning usually cause the far angle wavelet to be lower in frequency than the near angle wavelet. For this research, two wavelets were used, including a near angle wavelet ranging from 0 to 45° and a far angle wavelet ranging from 45 to 90°. The wavelet was then extracted using the statistical wavelet extraction which uses the seismic data volume to estimate a wavelet spectrum. This operation was carried out on the extracted wavelet using the angle-gather seismic volume as the input. An initial model was then created for the pre-stack inversion via the model process pane. This process makes use of the S-wave, P-wave, and density logs. Three models were generated at the end of this process. These models are P-impedance, S-impedance, and density model. A pre-stack inversion analysis was carried out on the 3-D pre-stack volume before inverting the entire seismic volume. The process was performed so as to apply inversion at the well location in order to verify the inversion parameters and optimize the seismic scaling. The entire 3-D pre-stack volume was then inverted. At the end of this process, the inverted density, inverted primary velocity (Vp), inverted secondary velocity (Vs), and the velocity ratio (Vp/Vs) was extracted for the purpose of predicting the pore pressure.

3.3. Pore-pressure prediction

3.3.1. Hydrostatic pressure estimation

The hydrostatic pressure is the pressure exerted per unit area by the weight of a static column of fluid, and it is a function of the height of the column of the fluid and the density of the fluid. The fluid in this case is fresh water with a density of 1.025 g/cc. The hydrostatic pressure at a given depth is estimated using Equation (2) and it is expressed in pounds per square inch (psi).

$$P_{\text{hydro}} = 0.433 \times z \times \rho_{\text{f}} \tag{2}$$

where:P_{hydro} is hydrostatic pressure in psi, z is depth in feet, ρ_{f} is density of fluid.

3.3.2. Estimation of overburden pressure

The overburden pressure was calculated by first generating the bulk density at each depth using the equation below:

$$\rho_{\text{zml}} = \rho_{\text{matrix}} - \left(\rho_{\text{matrix}} - \rho_{\text{top}}\right) * exp^{(-b * zml)} \tag{3}$$

where: ρ_{zml} is bulk density, ρ_{matrix} is density of matrix (2.65 g/cc), ρ_{top} is density at the surface (1.5 g/cc), b is coefficient of compaction (0.0005), *zml* is depth at mudline.

The bulk density was then multiplied with its corresponding depth to get the overburden pressure. It is measured in pounds per square inch (psi).

3.3.3. Establishment of normal compaction trend (NCT)

To establish the NCT for the well, the primary velocity (Vp) extracted from the seismic data and the primary velocity from sonic log was plotted against its corresponding depth respectively on a linear scale from a straight line relationship emerges. The top of the over pressured zone was determined by noting the depth at which the plotted points diverged away from the trend line in shale layers. The normal compaction trend was also established by plotting the interval transit time from the sonic log against depth on a linear scale. The top of the overpressure was then noted at the depth at which the plot diverges away from the trend line within the shale line interval.

3.3.4. Estimation of primary velocity in normal compacted shale (Vp_n)

The primary velocity (Vp) within the shale layer was estimated using the equation below:

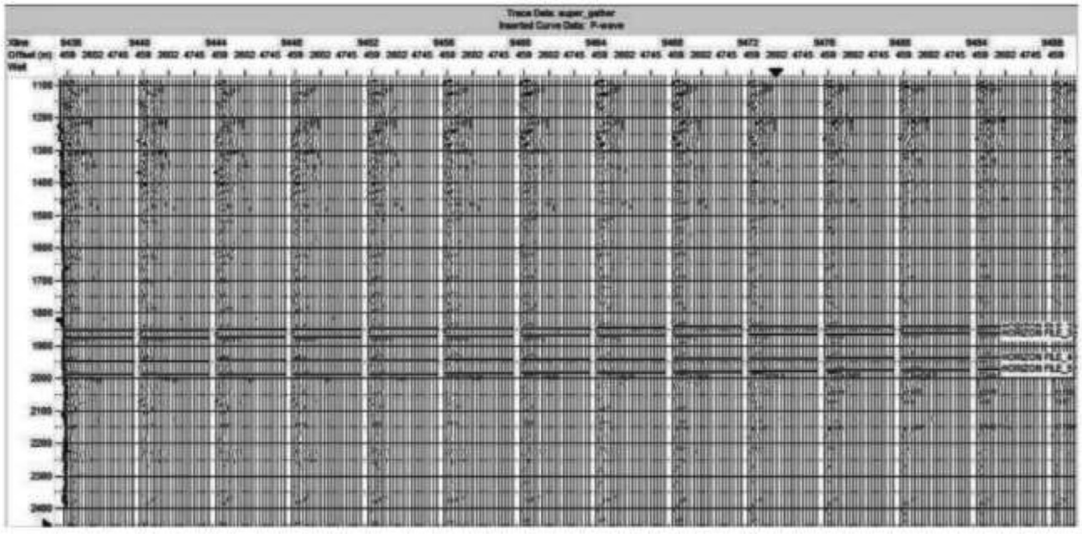

Fig. 8. Super gather and trim statics analysis on the seismic volume.

$$\frac{1}{Vp_n} = \frac{1}{Vp_{Matrix}} - \left(\frac{1}{Vp_{Matrix}} \frac{1}{Vp_{Top}}\right) * exp^{(-b*zml)} \quad (4)$$

where: Vp_n is primary velocity in normal compacted shale, Vp_{matrix} is primary velocity in shale matrix, Vp_{Top} is primary velocity at the surface, b is coefficient of compaction (0.0005), *zml* is depth at mudline.

3.3.5. Estimation of interval transit time in normal compacted shale (Δt_n)

The interval transit time within the shale layer was estimated using the equation below;

$$\Delta t_n = \Delta t_{Matrix} - (\Delta t_{Matrix} - \Delta t_{Top}) * exp^{(-b*zml)} \quad (5)$$

where: Δt_n is interval transit time in normal compacted shale,

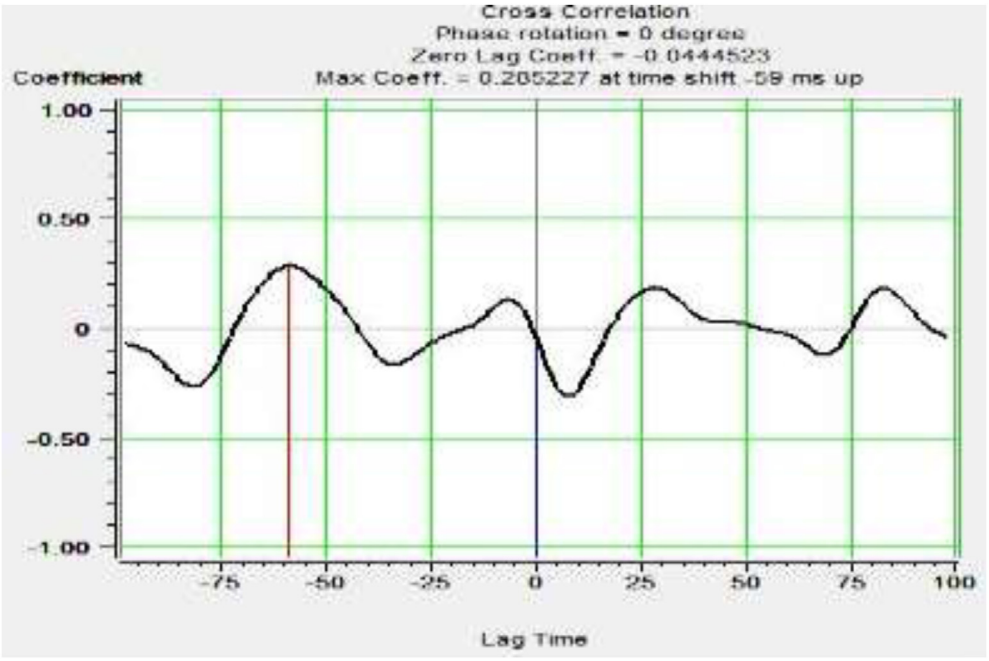

(a)

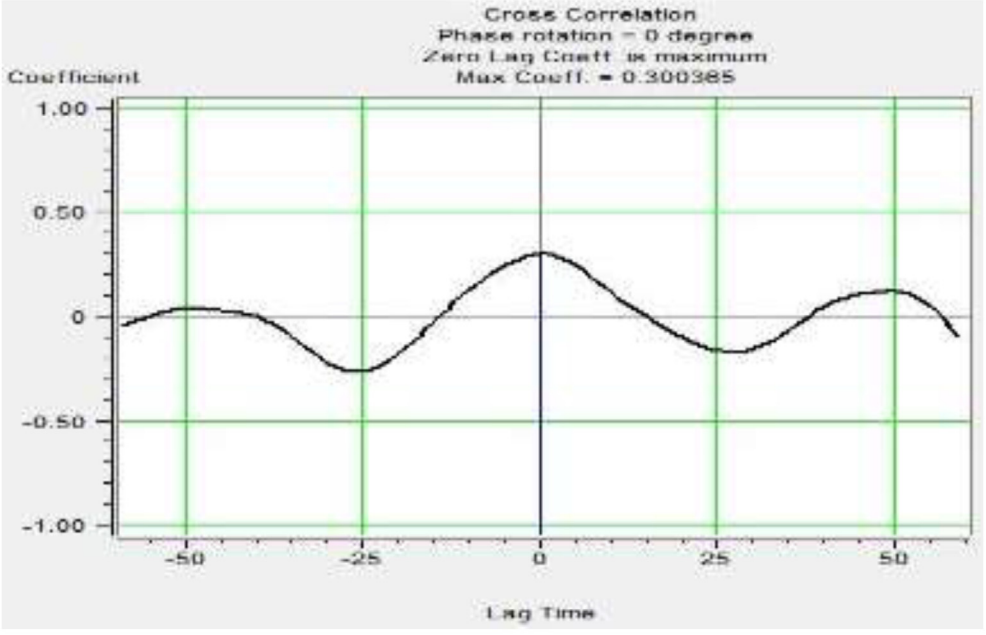

(b)

Fig. 9. (a) Wavelet cross-correlation panel before time shift (ms); (b) wavelet cross-correlation panel after time shift (ms).

Δt_{Matrix} is interval transit time in shale matrix (90 μs/ft), Δt_{Top} is interval transit time at the surface (200 μs/ft), b is coefficient of compaction (0.0005), *zml* is depth at mudline.

3.3.6. Pore pressure prediction from interval travel time

The pore pressure was predicted from the interval transit time using the Eaton's equation below;

$$PP = OBP - \left(OBP - P_{hydro}\right)\left(\frac{\Delta t_n}{\Delta t}\right) \quad (6)$$

where: *PP* is pore pressure, *OBP* is overburden pressure, P_{hydro} is hydrostatic pressure, Δt_n is interval transit time in normal compacted shale, Δt is observed interval transit time in shale.

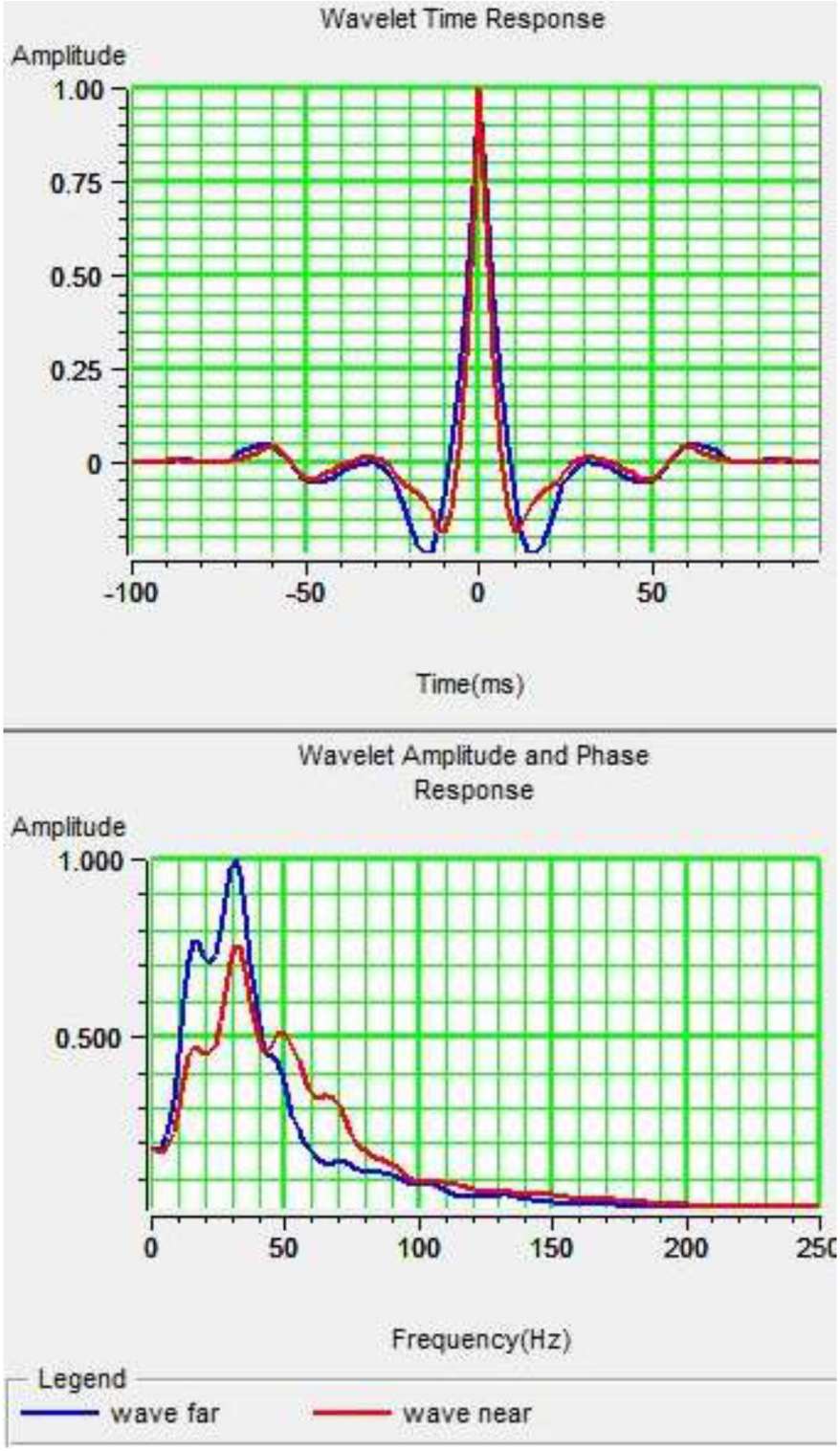

Fig. 10. Extracted wavelet, wavelet amplitude and phase response from the well.

3.3.7. Pore pressure prediction from seismic velocity

The seismic interval velocity extracted from the 3D pre-stack seismic volume through the inversion process within the study area was used for this study. Other data used include the hydrostatic pressure; lithostatic pressure; and normal compaction trend.

The pore pressure was predicted using the following equation:

$$PP = OBP - (OBP - HP)\left(\frac{V_p}{V_{pn}}\right)exp^b \quad (7)$$

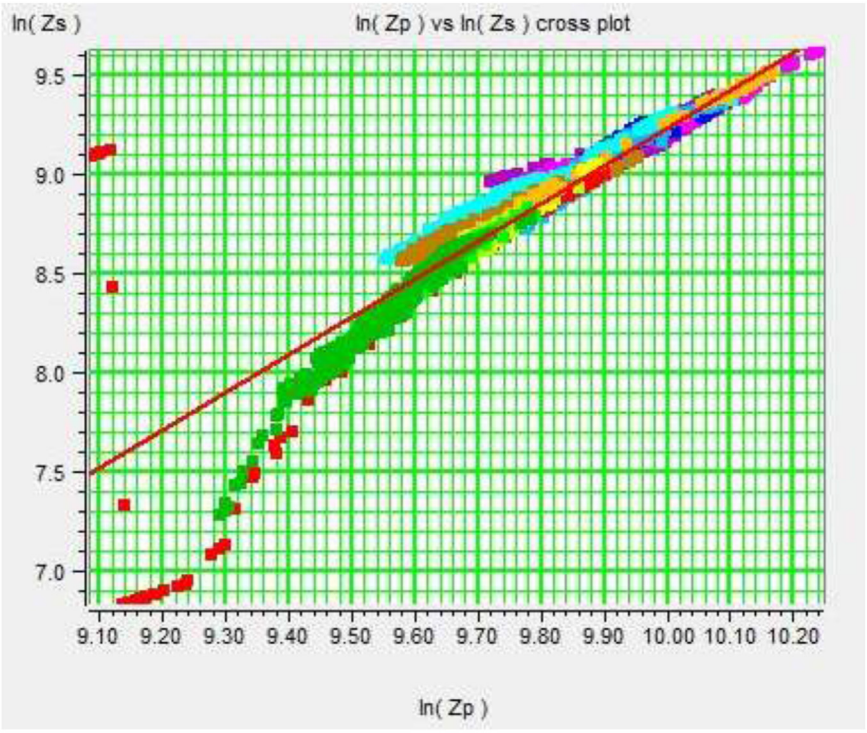

(a)

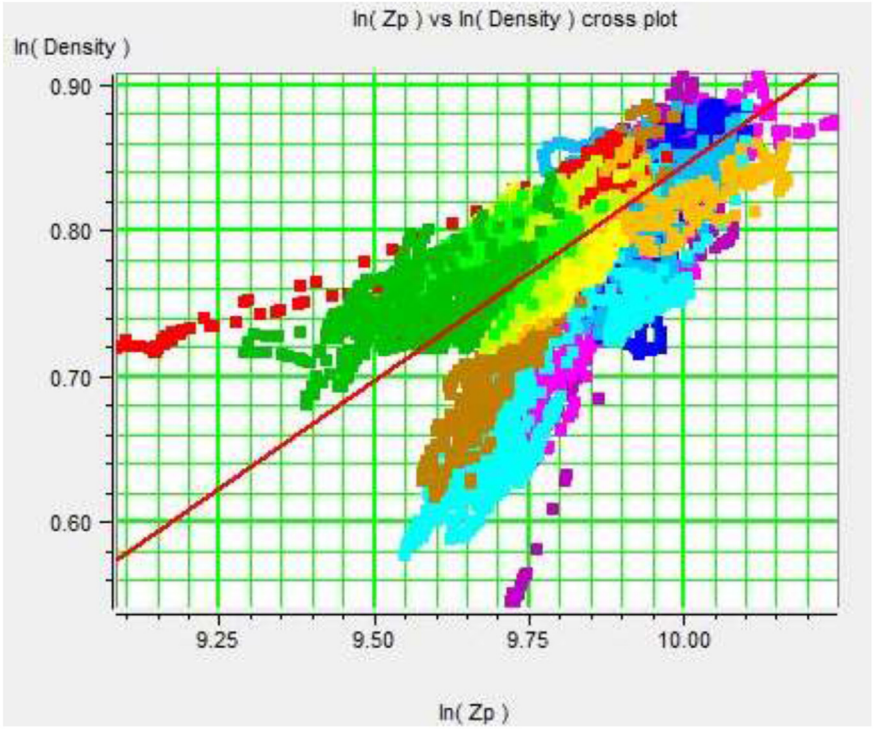

(b)

Fig. 11. (a) Plots of secondary impedance (Z_S) versus primary impedance (Z_P); (b) plots of density versus primary impedance (Z_P).

where: *PP* is pore pressure, *OBP* is overburden pressure, *HP* is hydrostatic pressure, V_p is P-wave velocity extracted from 3-D pre-stack seismic data and sonic log, b is local constant, V_{pn} is velocity of shale in normal compaction.

4. Results and discussion

4.1. AVO analysis

4.1.1. AVO modeling

Composite logs (Fig. 4) such as gamma-ray, P-wave, density and neutron-porosity logs were observed. S-wave was calculated from the P-wave using the Castagna's equation which was then used to generate an offset dependent synthetic for AVO modeling analysis. Poisson ratio log was computed from the extracted S-wave log. However, the computed Poisson ratio log at this stage is not the expected final Poisson ratio log since the Castagna's equation is only valid for wet background shale. The log chart of the density and neutron-porosity logs (Fig. 4) show that the sand is gas bearing reservoir, which totally validating that the computed Poisson ratio logs from the Castagna's equation was not the final. Seismic wavelet (Fig. 5a and b) were extracted from the pre-stacked seismic data to generate the offset dependent synthetic alongside with the P-wave, density, and computed S-wave logs. This wavelet is zero-phase and has a dominant frequency of about 30 Hz, which is determined from the seismic data, but this does not imply that the seismic data is at the zero-phase. The zero-offset dependent synthetic (Fig. 6) was then generated and correlated to the original seismic. It was observed from the correlation that there was a match between the zero-offset dependent synthetic and the seismic. The Zoeppritz equation was then used to generate reflection coefficient amplitude at each interface which was used to model the synthetic, so as to increase its frequency. The horizons (Fig. 7a and b) were mapped via the synthetic.

4.1.2. AVO processing

The seismic CDP gathers loaded were processed through the super gather process. The super gather was used mainly to increase the effective signal to noise ratio, while maintaining the AVO amplitude information. From the result (Fig. 8), it was observed that the seismic volume was much clearer and visible than the original seismic volume. On applying the trim statics, it was also observed that the hyperbolic wiggle shape observed initially on the seismic volume had been corrected and had become flat, through the process known as gather flattening. The seismic wiggles as well as the mapped horizons were flat (Fig. 8). Pre-stack inversion was actually operated in the incident angle domain, so the gathers were converted from offset to angle. From the angle-gather operation result, each input sample was mapped to its corresponding incidence angle.

4.1.3. AVO inversion

Fig. 9 is the correlation panel of the wavelet generated initially from the AVO modeling. It was observed from the wavelet correlation panel (Fig. 9a) with a very low correlation (4%) at the zero-phase. This was due to the fact that the time shift had not been applied to the wavelet generated. It was also observed that the wavelet shows a strong peak at 59 ms lag time. This indicates that a time shift of 59 ms is required to improve the fit. On applying the time shift of 59 ms to the wavelet, the new wavelet correlation panel (Fig. 9b) shows that the zero lag coefficient was at its maximum which was 30%. This indicates that there is a good correlation between the extracted synthetic and the seismic trace. Fig. 10 shows the wavelet extracted from the well, with its strongest peak at time 5 ms, which assisted in determining the phase of the seismic. It was also observed that the average phase response of the wavelet is −26°. The cross-correlation panel of the wavelet shows that the maximum correlation after applying the time shift is 32%. The pre stack inversion parameters such as primary impedance,

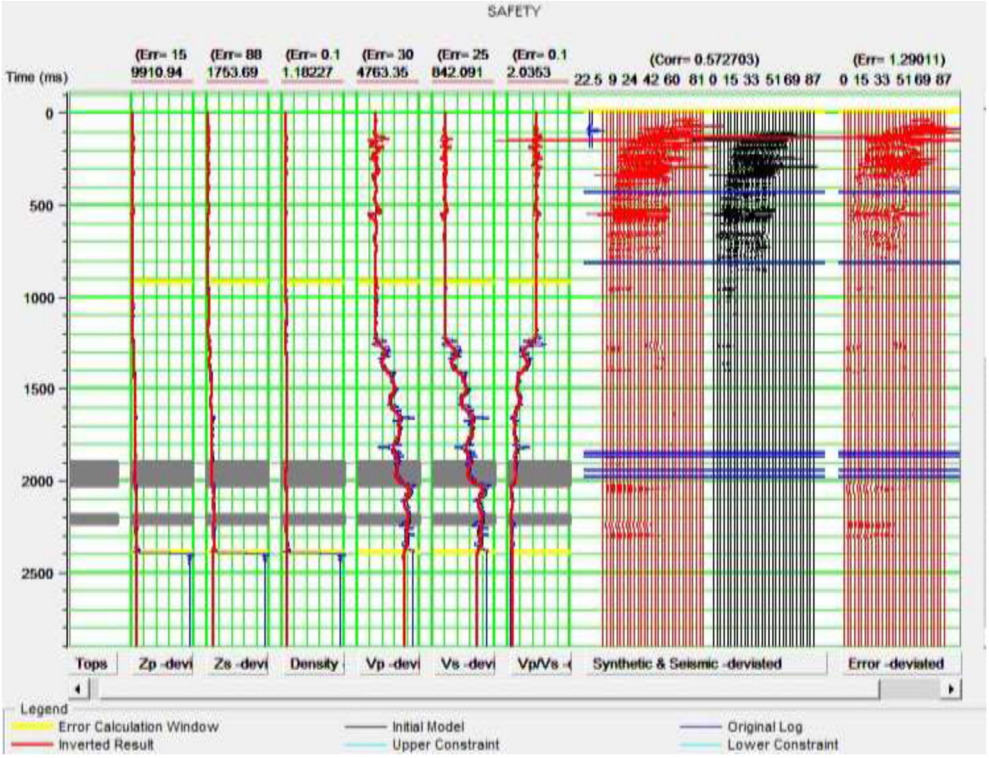

Fig. 12. Inversion analysis.

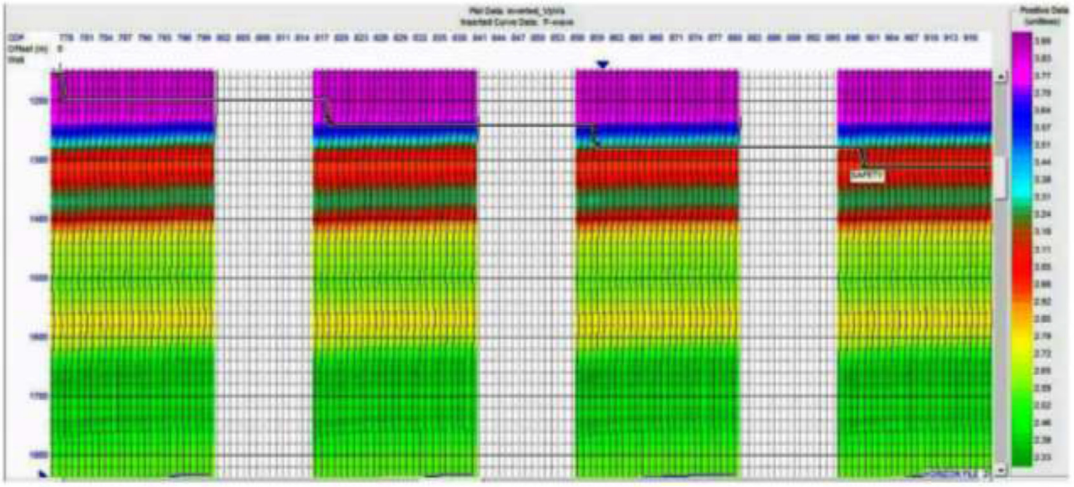

(a)

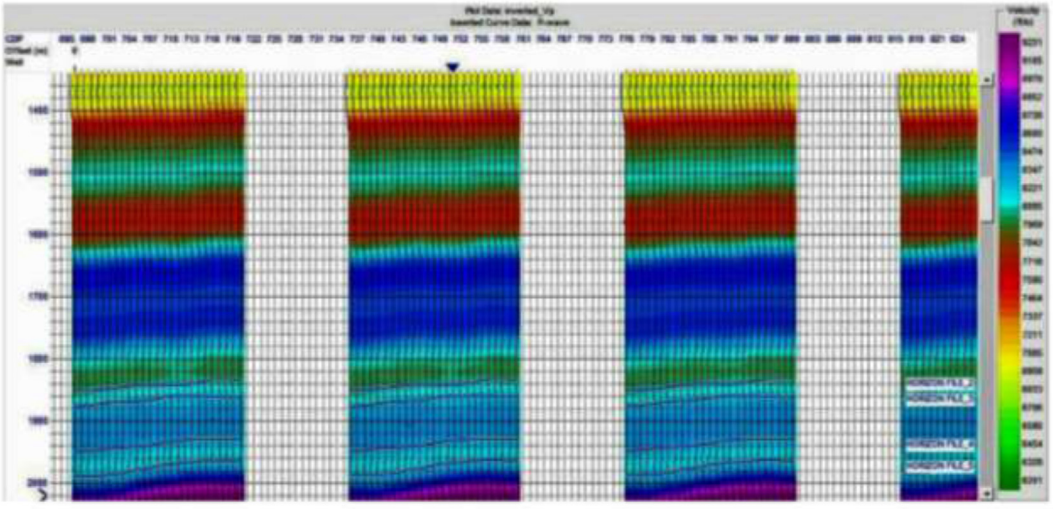

(b)

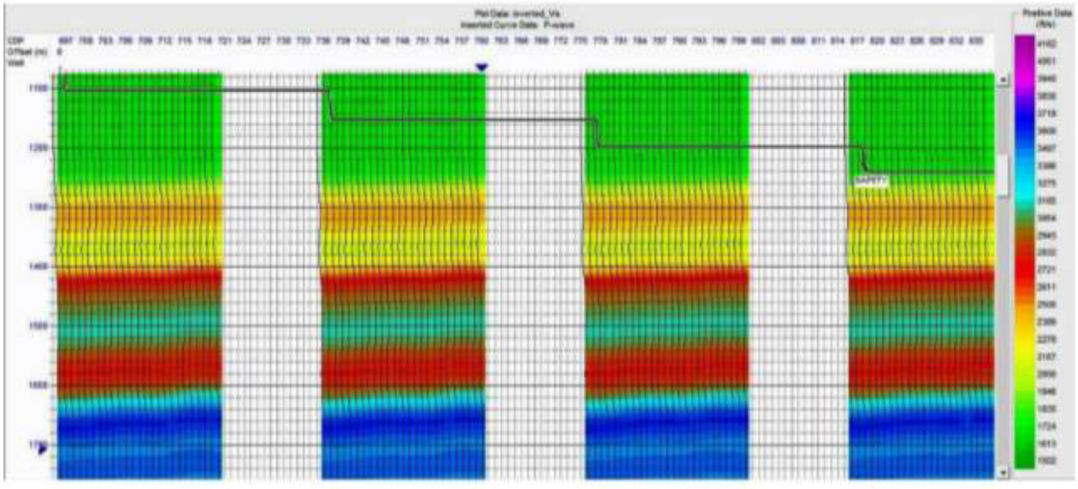

(c)

Fig. 13. Results of the inversion analysis (a) Inverted V_p/V_s; (b) inverted V_p; (c) inverted V_s.

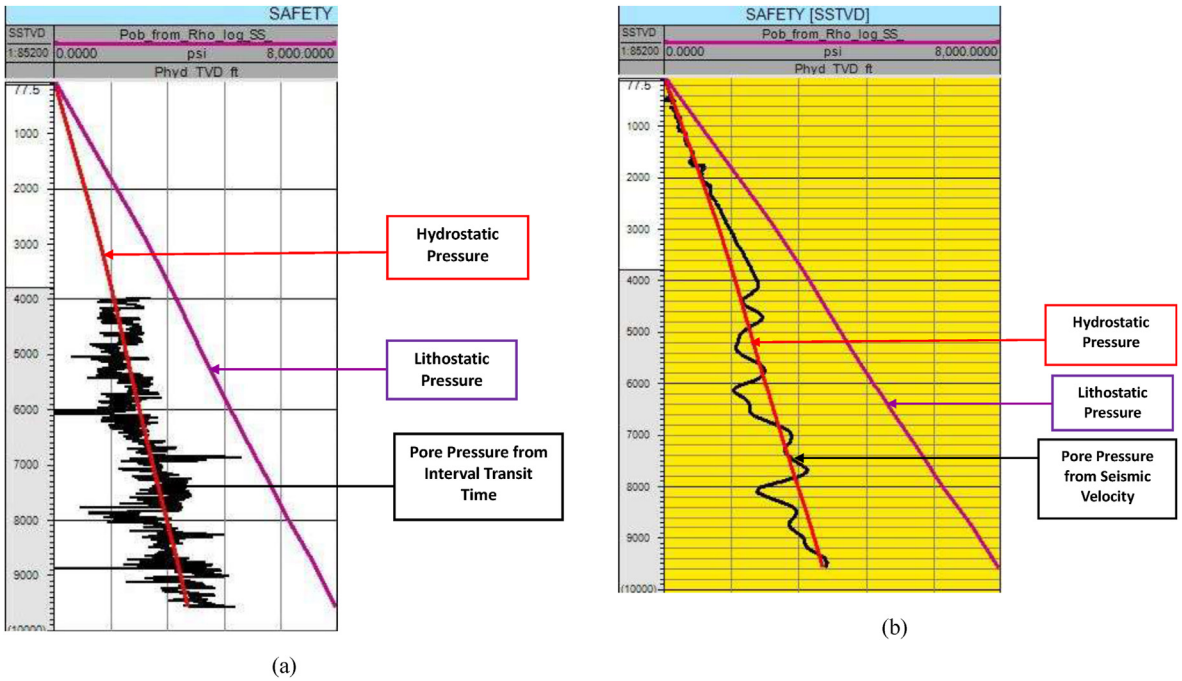

Fig. 14. (a) Pore pressure estimated from the interval transit time; (b) pore pressure estimated from the seismic velocity.

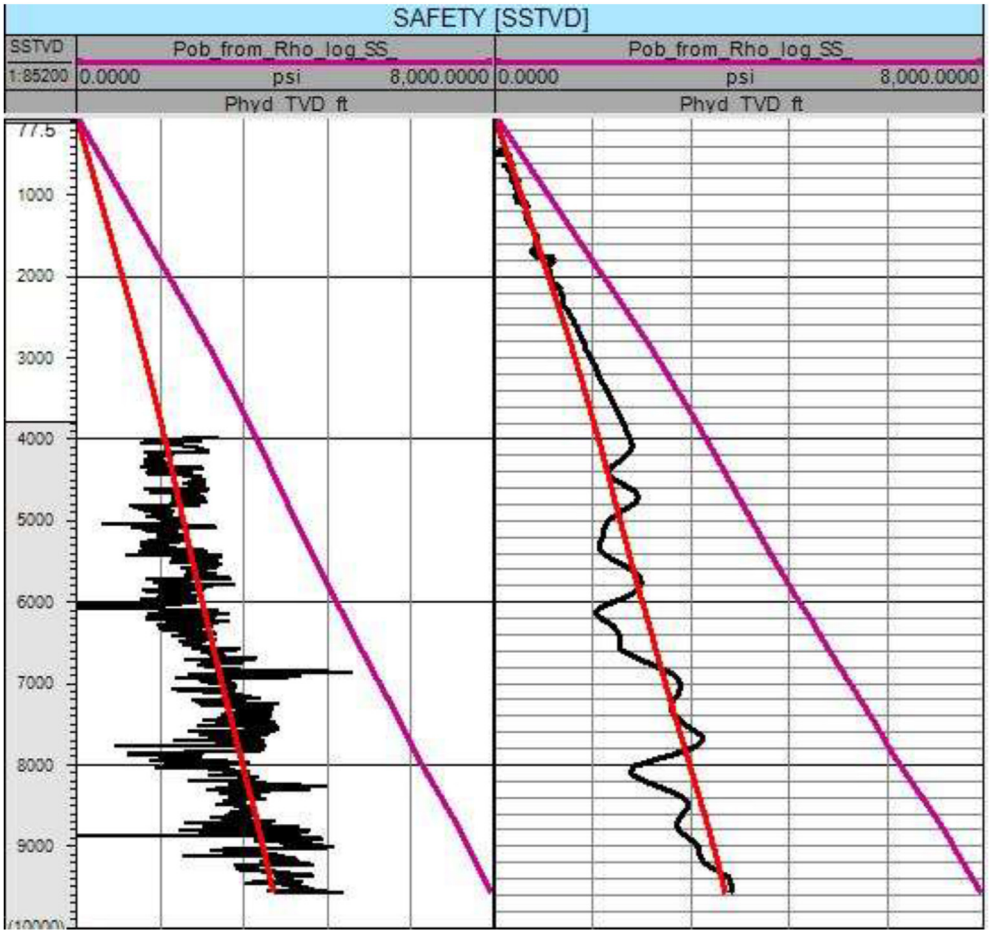

Fig. 15. Comparison between pore pressure predicted from the seismic velocity and pore pressure predicted from the interval transit time.

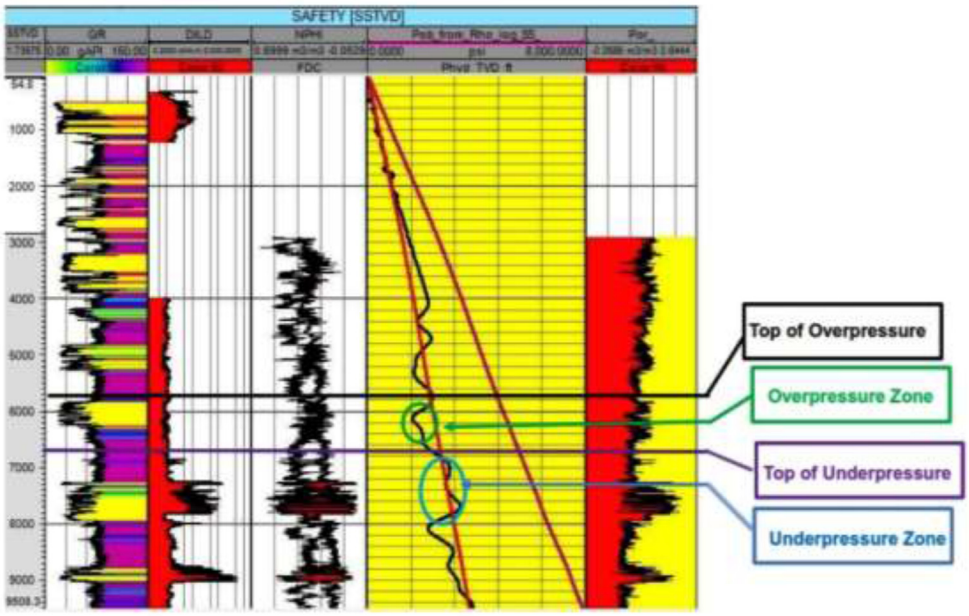

Fig. 16. Plots of Gamma ray, Resistivity, Density, Neutron Porosity, Pore pressure from Seismic Velocity, Hydrostatic Pressure, Lithostatic Pressure and Porosity.

secondary impedance and density impedance were generated. These serves as the main parameters that control the inversion.

They also help to control the background relationship and stabilize the inversion. Fig. 11a; shows plots of secondary impedance (Z_S) versus primary impedance (Z_P) and Fig. 11b, shows density versus primary impedance (Z_P). The assumption in this process is that, in the absence of hydrocarbons, there is a roughly linear relationship between these variables. The red lines indicate the current linear trend, which was manually positioned through the points to give a perfect trend. The process of controlling the background relationship for inversion stability before the final inversion process, a background smoothening of wet sands and shales was

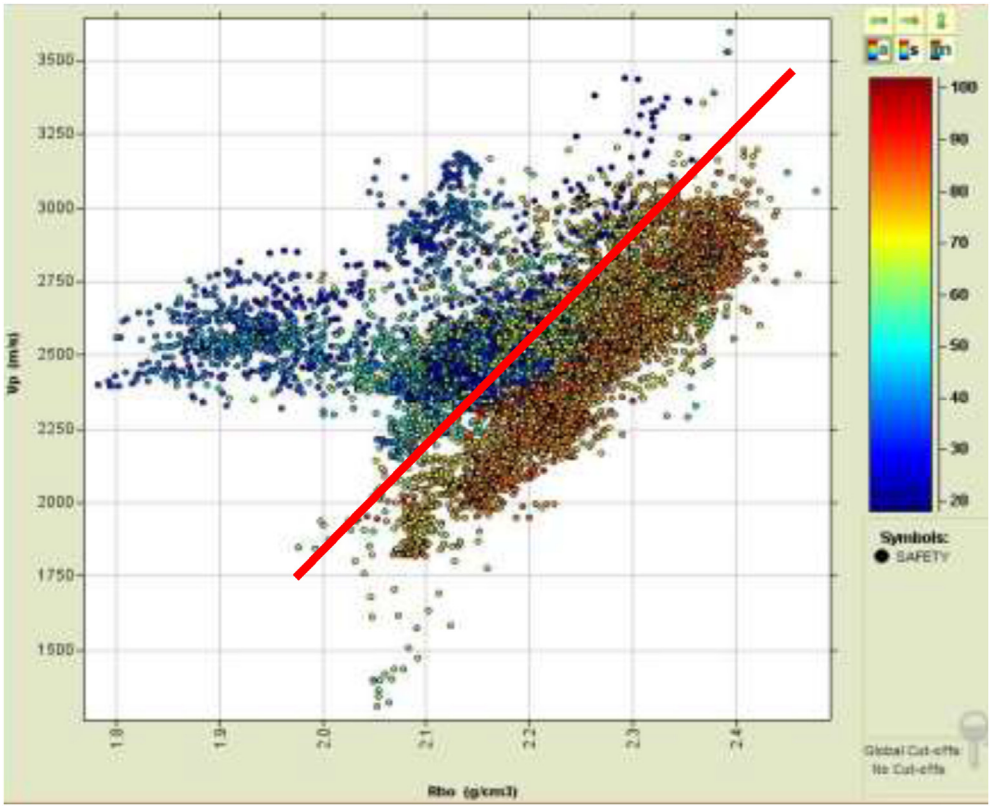

Fig. 17. Velocity versus density cross-plot.

done by considering the background V_s/V_p ratio value at 0.5.

Fig. 12 is the result of the final inversion analysis at the well location. Two important criteria were used to verify that the inversion parameters were optimum. The first was the error plot on the right hand side of the figure. It was observed from the figure that there was no consistent residual energy. From the observation, it can be concluded that the resulting inverted logs model the data. The second criterion used was the quality of the fit between inverted logs and the original logs. It was also observed that the inverted curve showing a very good correlation with the filtered log.

The inversion analysis was then applied to the entire seismic volume to give inverted velocities results. Fig. 13a, b and c show results of inverted V_p/V_s ratio, inverted V_p and inverted V_s respectively that were gotten from the seismic volume. The seismic velocity (V_p) was extracted from the inverted V_p for pore pressure estimation.

4.2. Pore pressure estimation

Fig. 14a shows the pore pressure estimated from the interval transit time, while Fig. 14b shows the pore pressure estimated from the seismic velocity. It could be observed that the pore pressure predicted from the seismic velocity has a better resolution than the pressure predicted from the interval transit time (Fig. 15). It was easier to identify the region that was over-pressured and under-pressured from the pressure predicted from the seismic velocity. The hydrostatic pressure and lithostatic pressure was overlaid on the predicted pore pressure curve. The pressure within this field ranges from 14.7psi to 3916psi. Fig. 16 shows that the over pressure top was delineated at depth of 6855 ft. At this depth, it was observed that the pore pressure was greater than the hydrostatic pressure i.e., at this depth, a pressure of 3053psi and a corresponding hydrostatic pressure of 2722psi were observed. Depth of the over-pressured region ranges from 6855 ft to 7802 ft. The under pressure top was delineated at a depth of 7883 ft. At this depth, it was observed that the pore pressure was less than the hydrostatic pressure, i.e., at this depth, a pressure of 1093psi and a corresponding hydrostatic pressure of 3122psi were observed. Depth of the under-pressured region ranges from 7883 ft to 9288 ft. The over-pressured zone could be caused either by loading or unloading mechanisms. In order to confirm the cause of the overpressure within this zone, it was observed from the log signatures that porosity values within the over pressure zone ranges from 23% to 53% which could be considered as relatively high. This could be as a result of the fact that the pore fluid cannot be expelled rapidly, thereby causing the pore fluid to increase rapidly since they are no longer compacted, thus leading to overpressure. The pore pressure within this interval is high as a result of the buoyancy effect of the fluid within the reservoir. As a result of overpressure top which is directly above the reservoir top within the shale zone, drilling this reservoir vertically could not be suggested so as to avoid possible blow out.

4.3. Velocity vs density cross-plot analysis

From the overpressure mechanism analysis using velocity-density cross-plot method (Fig. 17), it was observed that the plot had a negative trend. It was also observed that the sonic velocity was decreasing with a corresponding increase in the density of the formation. This suggests that the only primary cause or mechanism of overpressure within this field could be disequilibrium compaction.

5. Conclusions

Abnormal pressure of sub-surface from amplitude variation with offset (AVO) velocities information has been investigated in this research work. The AVO inversion carried out for this field aimed at extracting the seismic velocity which was later used for predicting the pore pressure of the field. The pore pressure predicted using the seismic velocity gave a better resolution than the pore pressure predicted from the sonic log, which has assisted to delineate zones of over pressure and under pressure respectively. Pore pressure within this field ranges from 14.7psi to 3916psi. The depth of over-pressure zones ranges from 6855 ft to 7802 ft. The overpressure top was delineated at a depth of 6855 ft-it has a pore pressure of 3053psi and a hydrostatic pressure of 2722psi. This implies that the pore pressure is greater than the hydrostatic pressure. The depth of under-pressure zones ranges from 7883 ft to 9288 ft. The under pressure top was delineated at a depth of 7883 ft-it has a pore pressure of 1093psi and a hydrostatic pressure of 3122psi. This implies that the pore pressure is lower than the hydrostatic pressure. It could be concluded that the over pressure observed within the reservoir was as a result of buoyancy effect of the fluid within the reservoir. Also, from the velocity-density cross plot, it was observed that the primary cause or mechanism of over pressure within this field could be disequilibrium compaction.

Editor

In order to conform to the format of journal, the manuscript has been modified by the editor of the journal. Please see the attachment for the edited manuscript, and check it carefully after that, please upload this edited manuscript to the system.

(1) All equations have been edited through Equation Editor, please check it- *The equations are edited using equation editor*
(2) All figures have been re-edited, please make sure not change style of the figures- *Addressed*
(3) Most of references are revised according to style of the journal except this reference (Narciso, João., Soares, Amílcar., Costa e Silva, Matilde (2014), Pore Pressure prediction and modeling using seismic velocities: Instituto Superior Técnico, Universidade Técnica de Lisboa, Av. Rovisco Pais, 1, 1049-001 Lisboa, Portugal, pp. 1). Please confirm this reference, and the style of this reference should be revised according to the journal- *Removed (Unable to confirm)*
(4) Please cite more articles from Petroleum Research in your manuscript- *Addressed*

Acknowledgements

The authors are grateful to Mr. Awoniran, D. R. of the department of Remote Sensing and GIS of the Federal University of Technology, Akure, Nigeria, for helping in re-editing some of the figures.

References

Abiola, O., Eyinla, S.D., Adeduyite, E.T., 2016. Pore ressure gradient prediction using ell logs: a case study on Malcolm Field, offshore Niger Delta, Nigeria. Int. J. Petrol. Geosci. Eng. 4 (1), 58–65.

Abiola, O., Olowokere, M.T., Ojo, J.S., 2018. Sequence stratigraphy and depositional sequence interpretation: a case study of “George” Field, offshore Niger Delta, Nigeria. Petrol. Res. 3 (1), 25–32. https://doi.org/10.1016/j.ptlrs.2017.12.001.

Bowers, G.L., 2012. Detecting high overpressure. Lead. Edge 21 (2), 174–177.

Chopra, S., Huffman, A.R., 2006. Velocity determination for pore pressure prediction. Lead. Edge 23 (12), 1502–1515.

Deming, D., Cranganu, C., Lee, Y., 2002. Self-sealing in sedimentary basins. J. Geophys. Res. 107 https://doi.org/10.1029/2001JB000504.

Doust, H., Omatsola, E., 1989. Niger delta. In: Edwards, J.D., Santogrossi, P.A. (Eds.), Divergent/passive Margin Basins. AAPG, Tulsa, pp. 239–248.
Dutta, N., 2002. Geopressure prediction using seismic data: current status and the road ahead. Geophysics 67 (6), 2012–2041.
Gutierrez, M.A., Braunsdor, N.R., Couzens, B.A., 2006. Calibration and ranking of pore-pressure prediction models. Lead. Edge 25, 1516–1523.
Hospers, J., 1965. Gravity field and structure of the Niger delta, Nigeria, West Africa. Geol. Soc. Am. Bull. 76, 407–422.
Jiang, Youlu, Wang, Xin, Yu, Qianqian, Wang, Yongshi, Liu, Hua, Chen, Jing, 2017. Pressure field characteristics of petroliferous sags in Bohai Bay Basin:Implication for hydrocarbon enrichment. Petrol. Res. 2 (3), 199–208. https://doi.org/10.1016/j.ptlrs.2017.03.001.
Kaplan, A., Lusser, C.U., Norton, I.O., 1994. Tectonic Map of the World, Panel 10. AAPG, Tulsa.
Klett, T.R., Ahlbrandt, T.S., Schmoker, J.W., Dolton, J.L., 1997. Ranking of the World's Oil and Gas Provinces by Known Petroleum Volumes. U.S. Geological Survey, Reston, VA.
Kulke, H., 1995. Nigeria. In: Kulke, H. (Ed.), Regional Petroleum Geology of the World. Part II: Africa, America, Australia and Antarctica. Gebrüder Borntraeger, Berlin, pp. 143–172.
Li, Y., Jiao, M., Xu, H., 2007. High Resolution Pore Pressure Prediction Using AVO Inversion. CSEG/CSPG, Calgary.
Odunayo, F.B., Ehinola, O.A., 2010. Fault Analysis, Stratigraphic Discontinuities and 3D Structural Modeling of Tb-Field, Offshore Niger Delta. AAPG International Conference and Exhibition, Rio de Janeiro.
Sayers, C.M., Johnson, G.M., Denyer, G., 2002. Predrill pore pressure prediction using seismic data. Geophysics 67, 1286–1292.
Swarbrick, R.E., 2001. Challenges of porosity – based pore pressure prediction. https://doi.org/10.3997/2214-4609-pdb.15.o-25.
Swarbrick, R.E., Osborne, M.J., 1998. Mechanism that generate abnormal pressures: an overview. AAPG Memoir. 70, 13–32.
Tingay, M.R.P., Hillis, R.R., Swarbrick, R.E., Morley, C.K., Damit, A.R., 2009. Origin of overpressure and pore-pressure prediction in the Baram province, Brunei. AAPG (Am. Assoc. Pet. Geol.) Bull. 93 (1), 51–74.
Tuttle, M.L.W., Charpentier, R.R., Brownfield, M.E., 1999. The Niger Delta Petroleum System: Niger Delta Province, Nigeria, Cameroon, and Equatorial Guinea, Africa. U.S. Geological Survey, Reston, VA.